Reviews
doi.org/10.1002/batt.202000228

Chemistry Europe
European Chemical Societies Publishing

Fe-Based Mesoporous Nanostructures for Electrochemical Conversion and Storage of Energy

Lemma T. Tufa,[a, b] Birhanu B. Gicha,[a] Hui Wu,[c] and Jaebeom Lee*[a, d]

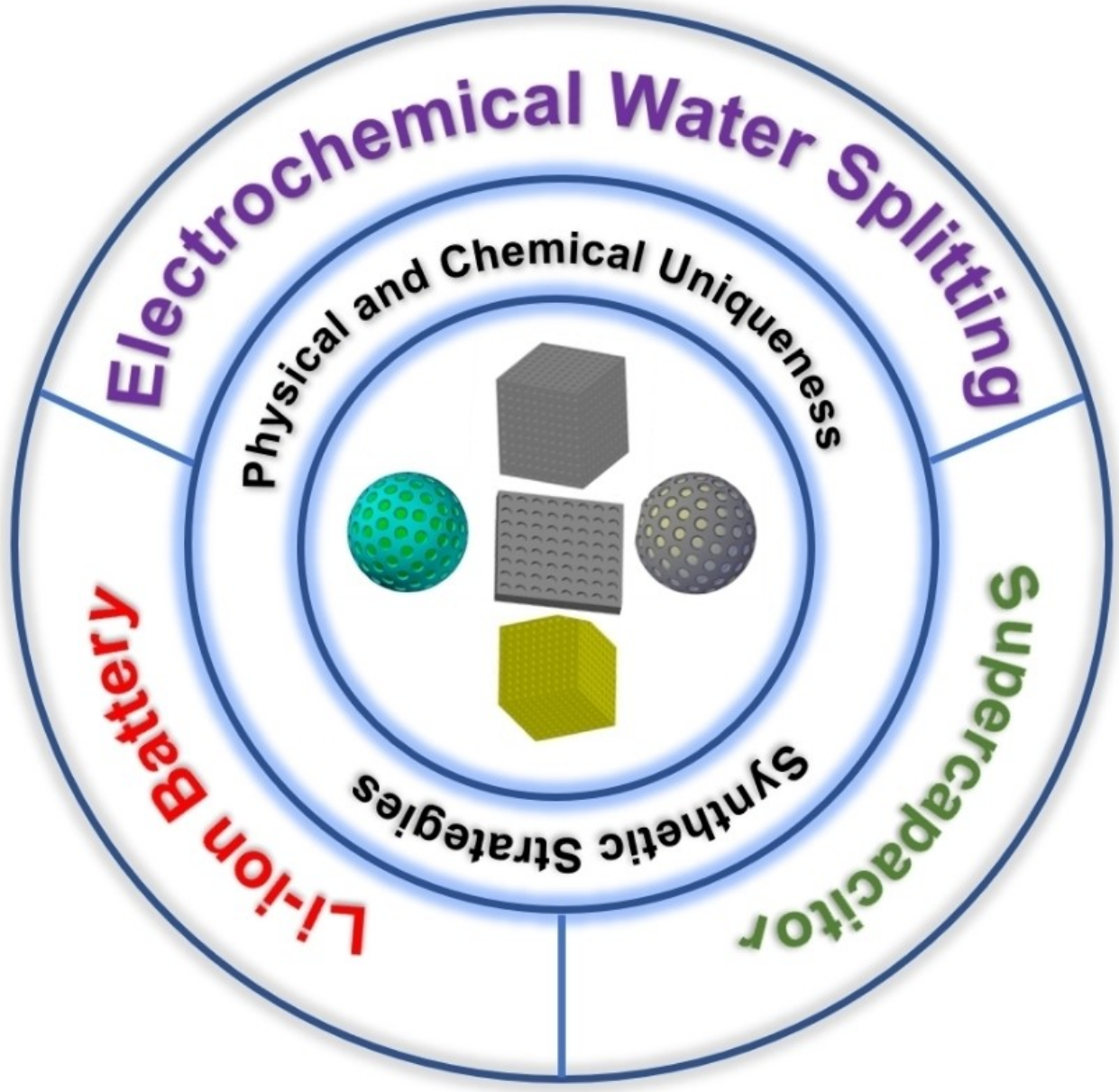

Decarbonization of the global energy system requires a coordinated effort towards disruptive technology of renewable energy conversion and storage (ECS) that can be potential to secure and diversify energy systems by increasing efficiency of conversion and storage of intermittent energy sources. Porous nanostructures have been newly reported as a promising class of most effective materials for this purpose because of their unique advantages in terms of large surface-to-volume ratios, surface permeability, and void spaces. These offer abundant active sites for ultimate electrochemical activities by the shortening pathway of mass/charge transport. Particularly, Fe-based mesoporous nanostructures (mp-FeNSs) have been recently fascinating. Iron is a principal active center in nanocomposites and has high industrial suitability for next-generation technology owing to its environment friendliness, abundance, and low cost. In this review, crucial technical advances related to mp-FeNSs that have occurred during 2016–2020 are summarized in terms of synthesis, structural design strategy, and ECS applications such as water electrocatalysis, Li-ion batteries, and supercapacitors. This review is supportive for potential readers to obtain general and professional information in this field since Fe-based energy materials are exclusively introduced in the article including a fundamental understanding of electrochemistry and related technologies in detail.

1. Introduction

The increase in demand for energy services coupled with the rise of environmental awareness has driven the research effort to search for alternative, green, and sustainable energy sources. On the other hand, renewable energy sources have the potential to satisfy the growing demand while also addressing environmental concerns. However, their widest potential has been constrained by their intermittent nature. One of the most effective strategies at advancing the contribution of renewable energy is through developing large-scale energy conversion and storage (ECS) system.[1] In the past two decades, researchers have made tremendous efforts to boost ECS technologies. For energy conversion technology, efficient redox catalysis has offered an important avenue in using renewable energy to process fuels. For instance, water electrocatalysis is an effective and clean technology and known by a generation of high purity hydrogen.[2] Despite their advantages, the wider applications of these technologies are still challenging due to their high cost, unsatisfactory duration, and operation difficulties, which are ultimately related to the severe nature of the materials problem. For energy storage technology, Li-ion batteries (LiBs) are essentially growing energy storage devices dominating the markets of portable electronic goods. Dating back to the 1970s, Li metal was used as anode material for rechargeable batteries offering the largest specific storage capacity.[3] The progress is promising where a LiB can generate an energy density of 260 $W\,h\,kg^{-1}$ at 700 $W\,h\,L^{-1}$ within a cell level.[4] The performances of LiB depend largely on the inherent properties of electrode materials and electrolyte solutions.[5] Furthermore, supercapacitors (SCs), another type of energy storage device, have also gained attention because of their high power density and lasting life cycle. SCs can provide up to 100–1000 times higher power density than normal LiBs.[6] However, the formation of an electrical double layer due to electrostatic storage of charges in electrodes leads to generating low energy density. To overwhelmed low energy density production, high surface area and specific pore sizes are required.[7]

Owing to their ability to absorb and interact with guest species on their outer and inner surfaces, and in the pore spaces,[8] porous nanomaterials, in particular, mesoporous nanostructures are attracted in ECS. International Union of Pure and Applied Chemistry (IUPAC) classified porous materials into three categories according to their pore sizes: microporous ($<$ 2 nm), mesoporous (2–50 nm), or macroporous ($>$ 50 nm). Among the various ECS materials, mesoporous nanostructures (mp-NSs) with pores size 2–50 nm have been reported as a promising class due to their structural advantage in terms of large surface-to-volume ratio, surface permeability, void spaces that offer abundant active sites, and fast mass/charge transport.[9] In particular, mp-NSs have been reported to be fit for ECS because of the confinement ability and cavities that are important for loading guest species.[10] Since the first report on mp-silica in the 1990s, different mp-NSs and compositions have been investigated, in which most cases, mp-NSs have been synthesized using soft/hard templates[11] or template-free[12] processes.

Iron-based nanomaterials have recently received increased attention as a promising material for ECS devices because of their earth-abundance, cost-effective, high chemical and thermal stabilities, low toxicity, and environmental-friendly properties.[13] Owing to their thermal stability, iron incorporation is highly preferred to mitigate oxygen release as a mechanism of minimizing thermal runaway in LiBs.[14] Iron is the center for biomimetic complex for activation because it has very rich redox properties for activation of O_2 in the biological system.[15] As a result, iron-based compounds can be used in the electrocatalysis of the oxygen evolution reaction (OER).

[a] Dr. L. T. Tufa, B. B. Gicha, Prof. J. Lee
Department of Chemistry
Chungnam National University
Daejeon, 34134, Republic of Korea
E-mail: nanoleelab@cnu.ac.kr
[b] Dr. L. T. Tufa
Department of Applied Chemistry
Adama Science and Technology University
P.O.Box 1888, Adama, Ethiopia
[c] Dr. H. Wu
Department of Cogno-Mechatronics Engineering
Pusan National University
Busan 46241, Republic of Korea
[d] Prof. J. Lee
Department of Chemical Engineering and Applied Chemistry
Chungnam National University
Daejeon, 34134, Republic of Korea

doi.org/10.1002/batt.202000228

However, poor cycle stability and low electrical conductivity are two major demerits plaguing iron-based materials for the selection of material for ECS.[16] Doping of iron nanomaterials with a nickel or cobalt-based catalyst has hurdled over these obstacles to dramatically improve electrocatalytic activities.[17] Yang *et al.*[18] designed and synthesized Fe-based anodes for the next-generation wearable Ni–Fe batteries. In their study they described fabrication of sulfur-doped Fe_2O_3 nanowire arrays (S–Fe_2O_3 NWAs) grown on carbon nanotube fibers (CNTFs) as an innovative anode material (S–Fe_2O_3 NWAs/CNTF). The S-doping in Fe_2O_3 dramatically reduced the bandgap from 2.34 to 1.18 eV and thus enhanced electronic conductivity.

In addition, nanomaterial design has appeared as a promising key to these important issues in LiBs and SCs.The generation of an active catalytic site is important for the development of Fe in energy-related applications. The specific surface area and pore structure of an iron composite affect the density of active sites and determine the accessibility of a three-phase interface transport path for the electrocatalysis of oxygen reduction reaction (ORR) relevant species.[19] According to the Raman spectroscopy, X-ray absorption fine structure, and Mossbauer spectroscopy results, Fe is the principal active center in nanocomposites used for ECS.[20] Furthermore, Fe-based mp-NSs (mp-FeNSs) have affluent localized *d*-electrons within the walls between pores, and they are endowed with unusual magnetic, semiconducting, electrical, and optical properties.[21]

In the past few decades, extensive research and although many high-quality reviews have been published, focusing on the preparation of iron-based nanomaterials and their applications in LIBs,[22] SCs,[23] and water splitting[24] no attention has been paid to mp-FeNSs. Therefore, this review aims to provide the reader great insight into a deeper understanding of the latest (2016–2020) design, synthesis, physical and chemical uniqueness of mp-FeNSs for electrochemical ECS technologies, where some of the synthesis techniques are obtained from our laboratory results.According to the google scholar search, more than 3000 publications and patents on mp-FeNSs have been published since 2016 in the ECS field. First, we review materials synthesis and physical and chemical uniqueness of distinguished mp-FeNSs, and then provide an overview in electrocatalysts, LiBs, and SCs. Finally, we summarize and suggest improved synthesis and engineering of mp-FeNSs for ECS and advance breakthroughs in the development of Fe-derived electrocatalyst.

2. Synthesis and Characterization of mp-FeNSs

2.1. Synthetic Strategies of mp-FeNSs

Various strategies for mp-FeNS synthesis, each having their own advantages and disadvantages, have been reported, classifying into as; 1) template-assisted (soft/hard templating) or 2) template-free method.[10b,25] The template-assisted strategy using soft or hard templating offers a facile way for the synthesis of mp-FeNSs.[26] Class of materials having flexible morphology including organic surfactants,[27] long-chain polymers,[28] and biological viruses,[29] are related to soft templates. Figure 2A shows a scheme to describe two typical synthesis methods. Meanwhile, the hard templates have relatively rigid structures; for example, inorganic,[30] organic[31]

Lemma Teshome Tufa received his Ph.D. degree in Nano Fusion Technology under the supervision of Prof. Jaebeom Lee at the College of Nano Science and Nano Technology, Pusan National University in 2019. He is currently an assistant professor at the chemistry department of Adama Science and Technology University (Ethiopia). His research interests include the development of nanostructures and their applications in nanoelectrochemistry with a focus on energy devices and biomedical science.

Birhanu Bayissa Gicha received his M. Sc. from the Center for Environmental Science, Addis Ababa University (Ethiopia). He is currently a Ph.D. candidate in the Department of Chemistry at Chungnam National University, Korea. His research interest includes nanomaterials synthesis and their energy storage and conversion applications, and environmental remediation.

Hui Wu completed his doctorate in Cogno-Mechatronics Engineering under the supervision of Prof. Jaebeom Lee at the Pusan National University (South Korea) in 2020. He is currently a postdoctoral fellow in the Laboratory of Advanced Materials at Fudan University with Prof. Xuebin Yu as his Principal Investigator. His current research interests include the design of novel nanomaterials for energy storage, especially for batteries, and the fundamental science of energy-storage systems.

Jaebeom Leeis currently a professor in the Departments of Chemistry at Chungnam National University (South Korea). He received his Ph.D. degree in Chemistry from Robert Gordon University in the United Kingdom in 2003. He worked as a research fellow at the University of Michigan, Ann Arbor, until 2007 and had worked at the college of nanoscience and nanotechnology, Pusan National University until 2018. His research interests include the fabrication and characterization of engineered assemblies of magnetoplasmonic nanomaterials and the synthesis of nanostructures for energy and biomedical applications.

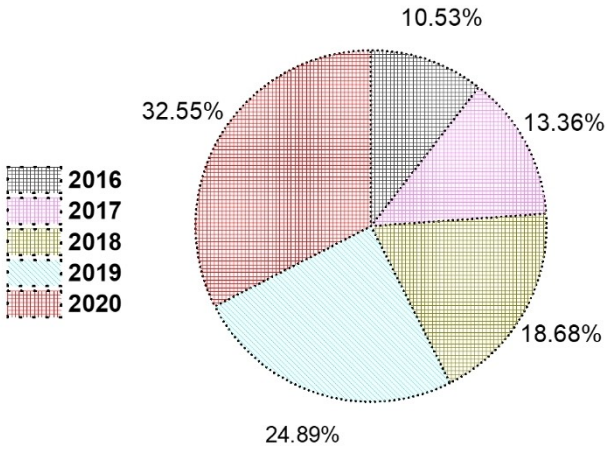

Figure 1. The mp-FeNSs applied in the ECS field published 2016–2020.

and organic-inorganic hybrid materials[32] are normally used as hard templates, typically including anodic aluminum oxide, silica, nickel foam, and polymer latex particles. In the soft-templating synthesis method, the composite is commonly made of the guest species that are co-assembled into ordered mesostructured and surfactant molecules. After removal of the soft template in the composite, the ordered mp-FeNSs with controlled open pores can be produced. In this synthesis method, the interaction between surfactant molecules and guest species is important for the development of well-controlled ordered mp-NS. Various morphologies and tunable pore designs of mp-FeNSs have been fabricated by many synthesis methods based on soft templating, including aqueous, non-aqueous, and hydrothermal processes.[33] However, it incurs a few challenges, such as low crystallinity, use of surfactants, and reaction condition-sensitive mesostructured formation under the reaction condition, which can be in complementary relation with hard-templating synthesis.

Meanwhile, the hard template-directed strategy has been a popular method for the preparation of mesoporous nanostructures owing to an ordered nanoarray structure, low sensitivity to reaction conditions, and high-quality and crystallinity products. The synthesis mechanism includes three main steps: template preparation, target material deposition, and template removal. For instance, Zhu *et al.*[34] fabricated ordered mp-Fe_3O_4 for atrazine ozonation through nanocasting technique using silica template as the hard template (Figure 2B). The material has demonstrated 154.2 $m^2 g^{-1}$ and 6.2 nm of surface area and pore size, respectively. In particular, mp-Fe_3O_4 has been used as an efficient catalyst to remove environmentally hazardous chemicals, such as atrazine. Although the hard-templating approaches are efficient for producing of mp-FeNSs, their shortcomings are distinct. One of the biggest problems is that the availability of the template which is difficult to be fabricated in the required size and shape. Furthermore, the production cost and template removal can be a major impedance.[35]

Structural-directing agents like surfactants, soft and hard templates are very important for the formation of hierarchical porous structures. Their additional removal step, however, makes difficulties in retaining the mesopores. Template-free methods are generally employed to produce materials with mp-structures. Multiple template-free syntheses of mp-NS have been reported, including solvothermal/hydrothermal,[36] organosilicon emulsion polymerization strategy,[37] pyrolysis.[38] A unique approach through solvothermal method with subsequent annealing was proposed for the synthesis of iron phosphide-phosphate (FeP–FeP_xO_y). Interestingly, particle-type of precursors has been used for the structural design of the final products. For example, iron oxy-hydroxide nanorods (NRs) as the precursors have been used to synthesize nanotubes of FeP–FeP_xO_y. The produced mp-FeP-FeP_xO_y composite nanotubes exhibited higher activity delivering a current density of 10 mA cm^{-2} at a low overpotential of 280 mV and small Tafel slope (48 mV dec^{-1}).[39] α-FeOOH and γ-Fe_2O_3 nanopowders as precursors were used to synthesizing reusable mp-α-Fe_2O_3 NRs. In particular, Hui *et al.* recently reported 1D magnetite NRs containing ordered mesocages.[40] The electrochemical activity of the ordered mp-magnetite NRs was compared with that of the Fe_3O_4 nanoplate. The redox potentials of magnetite ordered mesocages and Fe_3O_4 nanoplates were analyzed via a selective exposure of the crystal planes. The electrochemical characterization demonstrated that mp-ordered mesocage magnetite NRs were more electroactive than Fe_3O_4 nanoplates. These unique 1-dimensional shape of mp-FeNSs exhibited extraordinary electrochemical activity owing to high surface area with well-organized pore structure[41] and further research may be required to study different dimensional uniqueness.

Among recently developed highly porous nanostructures having the pore size between 0.4 and 6 nm, metal-organic frameworks (MOFs),[42] which are composed of metals connected by the organic linker is ideal for ECS applications.[43] Their exceptional porosity and thermal stability made them preferable over the traditional porous structure. Depending on the final properties and structures, MOFs can be synthesized via different synthesis techniques, such as electrochemical, microwave-assisted heating and ultrasonication, slow diffusion, mechanochemical, and solvothermal/hydrothermal.[44] Apart from iron site role in the inorganic catalyst, the iron single atoms in MOF configuration has been considerably investigated as an electrocatalyst. Chen *et al.* applied Fe atomic site with a single site attached on nitrogen, phosphorous, and sulfur-doped hollow carbon-based on zeolitic immobilized framework-8 (ZIF-8)@polymer composite via Kirkendall effect for ORR. The as-prepared electronic site tuned iron-active center supported on hollow carbon polyhedron and co-doped with sulfur, phosphorus, and nitrogen catalyst shows superior ORR activity in alkaline solution with a kinetic current density (J_k) of 71.9 mA cm^{-2} at 0.85 V, and a half-wave potential ($E_{1/2}$) of 0.912 V vs. reference hydrogen electrode (RHE).[45] Zhou *et al.*[18] developed a facile and cost-effective approach to directly grow MIL-88-Fe MOF-derived spindle-like α-Fe_2O_3@C on oxidized carbon nanotube fiber (S–α–Fe_2O_3@C/OCNTF). The S-α-Fe_2O_3@C/OCNTF electrode exhibited a superior specific capacitance of 1232.4 mF cm^{-2} at a current density of 2 mA cm^{-2} and an excellent rate capability with capacitance retention of 63%

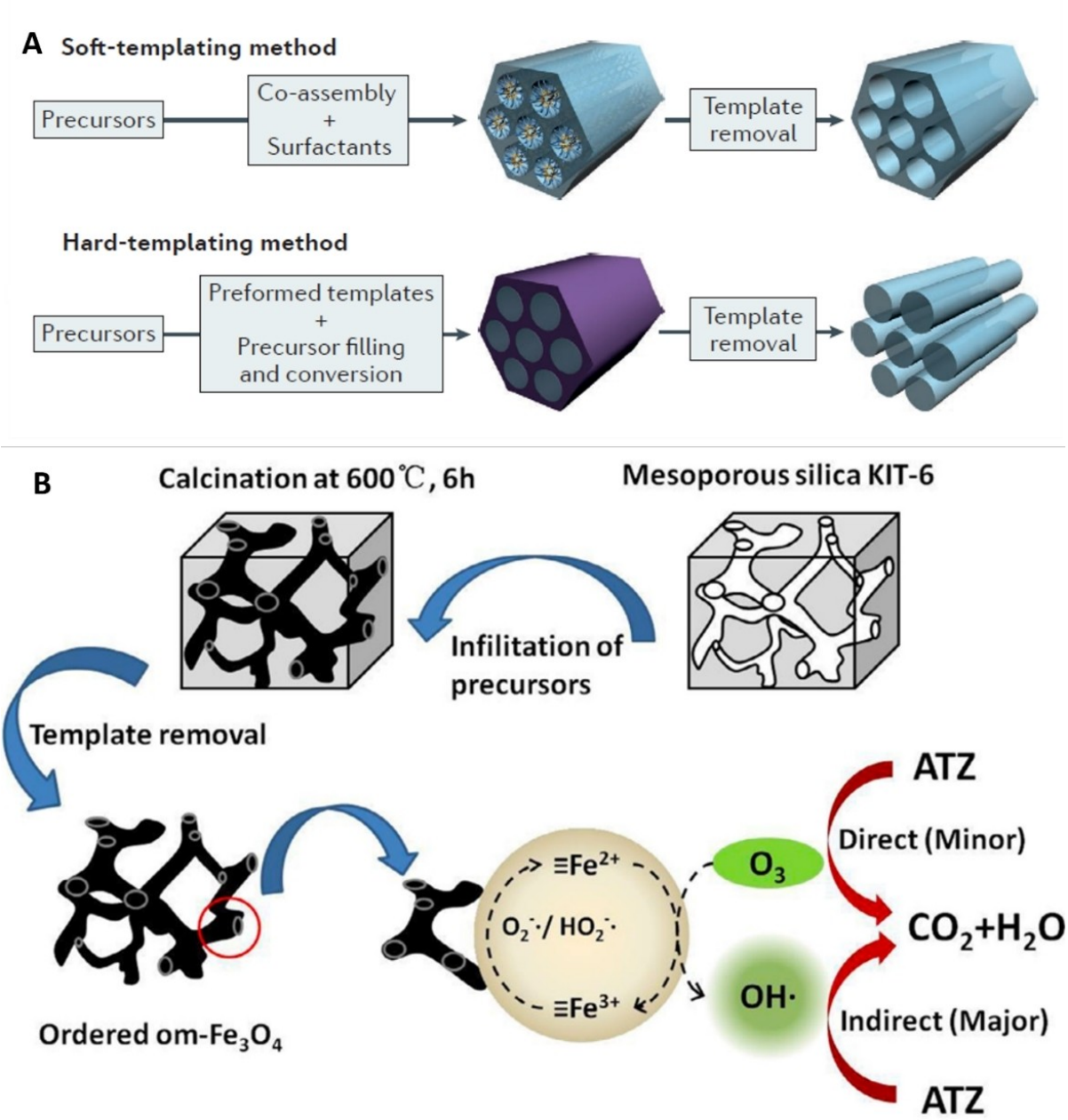

Figure 2. Soft and hard synthesis method. A) The principal methods for synthesizing mesoporous materials; soft-templating method and hard-templating method. Reproduced from Ref. [8] with permission. Copyright 2016, Springer Nature. B) Plausible mechanism of ATZ ozonation by ordered mesoporous Fe_3O_4. Reproduced from Ref. [34] with permission. Copyright 2017, Elsevier.

at a current density of mA cm^{-2}. The asymmetric supercapacitors composed of S-α-Fe2O_3@C/OCNTF anode and Na-doped MnO_2 nanosheets on CNTF possessed high specific capacitance of 201.3 mF cm^{-2} and an exceptional energy density of 135.3 μWh cm^{-2}. The improved electrochemical performances were obtained by the superior structure of MOFs derived α–Fe_2O_3@C, S–α–Fe_2O_3@C/OCTNF electrodes which increased electrical conductivity and specific surface area.

2.2. Physical and Chemical Uniqueness of the mp-FeNSs

The number of active sites and their specific intrinsic properties are the main factors to measure the performance of electrocatalytic materials.[46] Enhanced number of catalytically exposed active surface areas and active sites can be produced through increasing the porosity and decreasing the size of materials. Regulating the structural configuration and electronic structure increases the intrinsic properties of the metal active site.[47] The inherited property of Fe elements in the newly synthesized mp-FeNSs is an essential parameter, which can be supportive to fit into ECS devices. The addition of iron in binary or ternary

electrocatalysts has been shown to play a crucial role in the enhancement of catalytical activity toward energy conversion systems. Boettcher *et al.* showed that high electrocatalytic activity of $Co_{1-x}Fe_x(OOH)$ (i.e. ~100-fold higher for $x \approx 0.6$–0.7 than $x = 0$) is attributed to the presence of Fe ion while cobalt plays the role of transporting charge carriers.[17] Hung *et al.*[48] investigated the geometric site of cobalt and iron ions as well as *d*-band electrons configuration in Fe-doped cobalt oxides. They conclude that the bonding environment, structural conversion, and lattice geometrical site of metal ions govern the catalytic behavior. Görlin *et al.*[49] demonstrated the effects of conductive supports owing high surface-area and pH on the OER catalysis of the Fe–Ni oxyhydroxide catalyst in an alkaline solution, where *operando* differential electrochemical mass spectrometry tracked the catalyst redox state during the OER to observe a significant impact of Fe^{3+} centers on the Ni anodic and cathodic peak potential shift with a pH of an electrolyte. Chen *et al.*[50] reported that in the FeNi catalyst, Fe^{4+} species were detected, while in the Fe oxide electrocatalyst no Fe^{4+} was found, and revealed the synergic role of Fe and Ni in electrocatalytic water splitting. From many reports in the electrocatalytic reaction, Fe ions played a core role to enhance the catalytic effect. Among the iron compounds, Fe_3O_4 (magnetite) involves the transfer of eight electrons, giving an opportunity for the remarkable capacity of 925 mA h g^{-1}. Note that, battery-relevant electrochemistry is influenced by the crystalline size, electrode heterostructure, and morphology, mainly for crystallographically dense materials such as Fe_3O_4. In a LiB, lithiation first forms $Li_2Fe_3O_4$, and upon further lithiation $Li_xFe_3O_4$ is obtained ($x = 2$–5).[51]

A recent report indicated that the addition of iron single atoms in MOF-based nanomaterials promoted efficient electrocatalyst for ORR. Chen *et al.* fabricated a single-atom Fe/N-doped porous carbon. The resulting iron single atoms MOF showed excellent ORR activity in alkaline media with a $E_{1/2}$ of 0.87 V, performing better than the benchmark Pt/C electrodes. Furthermore, density functional theory (DFT) calculations confirmed that the high ORR activity is due to the high efficiency of the electron transporting from the single Fe atom to the adsorbed OH species.[52] To enhance the catalytic performance of single atom iron implanted N-doped porous carbon (denoted as Fe_{SA}–N–C), abundant single Fe sites, oriented mesochannels, hierarchal pores, and high conductivity are significantly important. Jiao *et al.*[53] prepared MOF with a high content (1.76%) single-atom Fe_{SA}–N–C via pyrolysis method. The outstanding ORR activity and robustness of Fe_{SA}–N–C were due to the presence of plenty of atomic Fe–N species catalytic active sites with hierarchical mesopores, which increased accessible active sites for mass and charge transport.

3. Energy Conversion Using mp-FeNSs: Electrochemical Water Splitting

3.1. Fundamental Concepts of Electrochemical Water Splitting

Among the clean energy conversion technologies, hydrogen production through electrochemical water splitting ($2H_2O \rightarrow 2H_2 + O_2$) is one of a promising generation of green and renewable energy source. Water-splitting technologies depend on a series of electrochemical reactions such as hydrogen evolution reaction (HER), OER, and ORR. One of the main problems for the overall water splitting is the sluggish kinetics of OER, which involves multiple steps of proton-coupled electron transfer.[54] The detailed reaction mechanisms of ORR, HER, and electrochemical metal peroxide path of OER in acidic and basic media are given in Table 1.[55] Theoretically, the minimum energy required for the catalytic decomposition of water is $\triangle G = 237.1$ KJ, that corresponds to an applied voltage of 1.23 V to overcome the thermodynamic energy barrier.[56] To defeat the kinetic barrier at a relatively low overpotential, cost-effective, and highly efficient catalysts are required.[57] Highly exposed active sites and fast charge/mass transport of the mp-FeNSs are particularly important for electrocatalytic reactions.

The most important kinetic parameters used to evaluate the electrocatalytic activity are overpotential (η), Tafel plots, stability, Faradaic efficiency, and turnover frequency (TOF). An overpotential (also called extra-potential) is the additional potential (beyond the minimum energy) required to drive a reaction at a certain rate.[58] It can be expressed as the difference between the applied potential (E) and the potential under equilibrium condition (E_{eq}). Choosing an efficient catalyst can minimize the activation overpotential, which is an intrinsic property of a given material.[59] Typically, an overpotential is

Table 1. Proposed reaction mechanisms for ORR, OER, and HER.[55]

Electrochemical reaction	In acid media	In alkaline media
ORR	$O_2 + 4H^+ + 4e^- \rightarrow 2H_2O$ $O_2 + 2H^+ + 2e^- \rightarrow H_2O_2$ $H_2O_2 + 2H^+ + 2e^- \rightarrow 2H_2O$	$O_2 + 2H_2O + 4e^- \rightarrow 4OH^-$ $O_2 + H_2O + 2e^- \rightarrow HO_2^- + OH^-$ $H_2O + HO_2^- + 2e^- \rightarrow 3OH^-$
OER	$M + H_2O \rightleftharpoons$ $M\text{–}OH + H^+ + e^-$ $2\ M\text{-}OH \rightleftharpoons$ $M\text{–}O + M + H_2O$ $M\text{–}O + H_2O \rightleftharpoons$ $M\text{–}OOH + H^+ + e^-$ $2\ M\text{-}OOH \rightleftharpoons$ $M\text{–}O + O_2 + H_2O + M$	$M + OH^- \rightleftharpoons M\text{-}OH + e^-$ $M\text{–}OH + OH^- \rightleftharpoons$ $M\text{–}O + H_2O + e^-$ $2MO \rightleftharpoons 2\ M + O_2$ $M\text{–}O + OH^- \rightleftharpoons$ $M\text{–}OOH + e^-$ $M\text{–}OOH + OH^-$ $\rightleftharpoons M + O_2 + H_2O + e^-$
HER	Tafel step: $H_2 \rightleftharpoons H_{ads} + H_{ads}$ Heyrovsky step: $H_2 \rightleftharpoons H_{ads} + e^- + H^+$ Volmer step: $H_{ads} \rightleftharpoons H^+ + e^-$	Heyrovsky step: $H_2 + OH^- \rightleftharpoons H_{ads} + e^- + H_2O$ Volmer step: $H_{ads} + OH^- \rightleftharpoons H_2O + e^-$

reported as a current density (j) reaching 10 mA cm^{-2}. The electrochemical activity of the electrocatalyst is usually obtained from linear sweep voltammetry (LSV) or cyclic voltammetry (CV). The Tafel plot is obtained from the polarization curve as a plot of log(j) vs. η and the slope of linear region of the below equation is used to compare electrocatalytic properties of the nanostructures.

$$\frac{d\log(j)}{d\eta} = \frac{2.303RT}{\alpha nF} \quad (1)$$

where j is current density, T is temperature, R is an ideal gas constant, F is Faraday constant, and n is the number of electrons transferred, where OER and HER have value of 4 and 2, respectively, and α is the charge transfer coefficient. From Equation (1), a catalyst with a high charge transfer has a small Tafel slope. The stability test is also one of the crucial parameters for checking the performance of the catalysts. Stability is usually measured with CV cycling at a rapid scan rate for 250–1000 cycles and chronoamperometry or chronopotentiometry for several minutes. The number of CV cycles and time measurement strongly depend on the nature of the nanomaterials. Faradaic efficiency is the efficiency of an electrocatalyst to transfer electrons involved in an electrochemical process. It can be calculated from the ratio of the experimentally produced O_2 amount (n_{O2}) to the theoretically produced O_2 amount ($n_{O2'}$).[60] At a constant oxidation current (I) within a given time (t) and assuming that the production of O_2 molecules consumes four electrons, Faradaic efficiency is given by Equation (2):

$$\frac{n_{O2}}{n_{O2'}} = \frac{4Fn_{O2}}{It} \quad (2)$$

TOF is one of quantitative measurements of the catalytic activity of nanostructures. It is defined as the number of O_2/H_2 evolved per unit time,[59] and is calculated using Equation (3).

$$\mathrm{TOF} = \frac{j\,(A)}{4Fn} \quad (3)$$

where, n is the number of moles of the active materials, and A is the area of the working electrode.

3.2. Electrochemical Water Splitting Using mp-FeNSs

In the essential aspect of electrochemical water splitting, reactions always occur at an electrode surface where various nanomaterials are decorated. For example, for the HER, a broad range of mp-NSs from precious metals (platinum group) to *3d* transition metals including Mn, Fe, Ni, and Co as well as their corresponding alloys have been explored for the conversion of H_3O^+(acid) and H_2O (alkaline) to H_2. Among these materials, mp-FeNSs with various structures and compositions have been reported as promising electroactive nanomaterials for efficient water-splitting. Reproduction of high efficiency in various Fe-based structures and their combinations with other (non)metals have been a recent research topic (Table 2). Kang *et al.*[61] fabricated a mp-NiO/$NiFe_2O_4$ multi-composite nanocage through monodispersed $Ni[Fe(CN)_6]_2$, that exhibited high OER activity delivering 10 mA cm^{-2} of current density at 303 mV applied overpotential, Tafel slope of 58.5 mV dec^{-1}, and cycling stability in the alkaline electrolyte at 60 mA cm^{-2} for 12 h. Yan *et al.*[62] prepared nonprecious mp-$MnFe_2O_4$ NR arrays for efficient water oxidation, possessing 10-fold higher water oxidation than that of commercially available 20 wt% Pt/C catalyst at 1.8 V_{RHE}. That is, the mp-structure that can provide an efficient electrolyte diffusion path induced the remarkable enhancement of electrolytic activities of OER. Furthermore, the doping of metals or non-metals that can enhance the electrochemical activity has been extensively reported. Wu *et al.*[63] reported a Co-doped Ni–Fe composite oxide mp-nanosheet array for water-splitting electrocatalysts.[117] A well-connected mp-nanosheet array provided numerous catalytic active sites and an open channel for electron and ion transport. In addition, the $NiFe_2O_4$ catalytic phase improves the catalytic activity, while Co^{2+} increases the electrical conductivity and Ni active sites at lower overpotential through charge transfer effects. A composition of $Co_{6.25}Fe_{18.75}Ni_{75}O_x$ and Co-doped NiO/$NiFe_2O_4$ metal oxide mp-nanosheet array showed outstanding OER performance delivering 10 mA cm^{-2} of current density at 186 mV applied overpotential. Moreover, the material exhibited high performance for HER performance, with a low overpotential of 84 mV to reach 10 mA cm^{-2}. The intrinsic electrocatalysis of a multi-component containing spinel-type mp-FeNSs is determined by the crystal structure, chemical composition, and oxidation state of the cations.[64] Although some of the Fe–Ni bi-functional nanostructures have shown sufficient OER activity, their major problems are still poor stability and electrical conductivity, which limit their industrial applications. Many researchers have tried to solve this problem through a synthesis technique and hybridization with conductive materials. Kumar and Bhattacharyya designed an OER and HER active electrocatalyst NiFe-oxide nanocube (NiFe-NC, about 200 nm).[65] The synthesized NiFe-NCs performed outstanding OER and HER activities with a low overpotential of 271 and 197 mV for OER and HER, respectively to reach at 10 mA cm^{-2}.

Table 2. Comparison of recent mp-Fe-based OER electrocatalysts in alkaline media at current density of 10 mA cm^{-2}.

Catalyst	Overpotential mV vs. RHE]	Tafel slope [mV dec^{-1}]	Electrolyte	Ref.
$Co_{6.25}Fe_{18.75}Ni_{75}O_x$	186	38.5	1 M KOH	[63]
NiO/$NiFe_2O_4$	303	58.5	1 M KOH	[61]
CoFe–Se–P	1440	108	0.1 M KOH	[73]
$NiFe_2O_4$	332	44	1 M KOH	[74]
NiO/α/y-Fe_2O_3	271	48	1 M KOH	[65]
$MnFe_2O_4$	315	~50	0.1 M NaOH	[62]
$Ni_{0.8}Fe_{0.2}$	206	64	1 M KOH	[75]
NiO/$NiFe_2O_4$	302	42	1 M KOH	[76]
$FeCoGaO_x$/Ni-foam	215	40.2	1 M KOH	[77]
NiCoS@CoFe	268	62	1 M KOH	[78]
$(FeO)_2.(MoO_2)_3/MoO_2$	200	70.3	1 M KOH	[79]
FeNiCoP	259	40	1 M KOH	[80]

The spherical NiFe oxide NPs with a similar composition showed overpotentials of 347 and 339 mV for OER and HER, respectively. It was probable that the superior OER and HER of NiFe-NC resulted from the exposure of active sites at the edges and vertices of the nanocubes (Figure 3A–C).

To further improve the performance of mp-FeNSs based oxygen electrodes, certain essential factors should be taken into account adequately, such as robust structure for long term electrocatalysis, desire electrical conductivity for fast electron transport, creating an abundant site by modifying with heterogeneous elements and engineering the nanostructures.[66] Accordingly, enhancing the electrical conductivity and surface area of mp-FeNSs by carbon materials have been widely adopted. Hong *et al.*[67] developed the modified nitrogen-doped mesoporous carbon (NMC) composited of a series of 2D transition metal selenides (MSe, M = Fe and/or Co) for OER/ORR. The NMC Oxygen Electrode with ultrathin 2D Iron/Cobalt Selenides showed excellent electrocatalytic performance with onset potential (1.52V, for OER) and $E_{1/2}$ (0.90 V, for ORR) even after 5000 accelerated durability test cycles at typical working potentials. Furthermore, Sun *et al.*[68] prepared the electrocatalyst composed of isolated single Fe atoms coordinated to graphitic carbon nitride ($g\text{-}C_3N_4$) dispersed on hierarchical porous N-doped carbon polyhedra (Fe-$g\text{-}C_3N_4$/HPNCPs) for ORR. The Fe-$g\text{-}C_3N_4$/HPNCP catalysts with various Fe contents were synthesized by first adsorption of iron nitrate nonahydrate ($Fe(NO_3)_3.9H2O$) and urea on meso SiO_2-coated-ZIF-8-derived hierarchical porous carbon particles, followed by thermally treating this product under an argon-gas atmosphere. The optimal Fe-$g\text{-}C_3N_4$/HPNCP-0.8 catalyst delivered superior electrocatalytic activity for the ORR in 0.1 M KOH electrolyte with a highly positive half-wave potential ($E_{1/2}$) of 0.902 V vs. RHE, 60 mV higher than the $E_{1/2}$ value of the commercial Pt/C catalyst (0.842 V), as well as high durability and strong tolerance to methanol. The experimental results revealed that the atomically dispersed Fe–N_2 sites played a key role in endowing the Fe-$g\text{-}C_3N_4$/HPNCP-0.8 catalyst with excellent ORR catalytic activity, while the hierarchical micro–mesoporous structure played an important role in

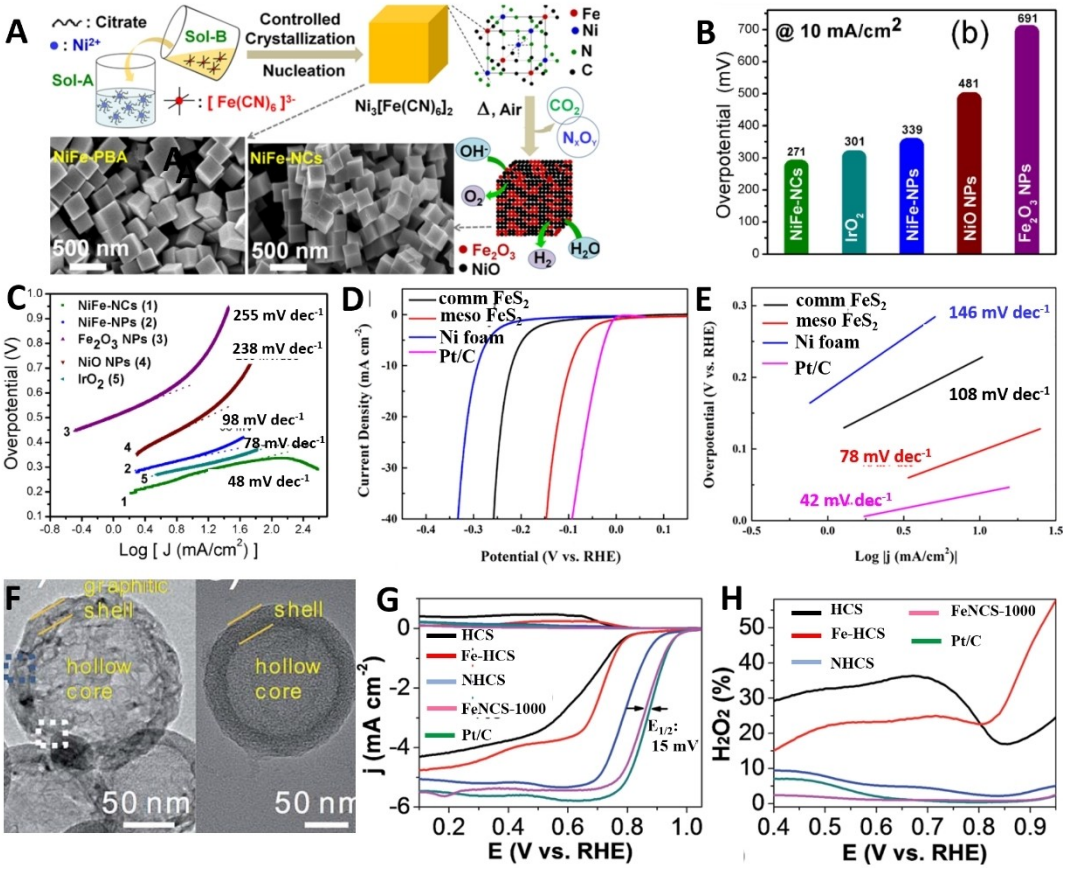

Figure 3. Electrochemical water splitting. A) Schematic of the formation of NiFe-Purussian blue analog-derived porous NiFe-nanocubes (NCs) and NiFe-nanoparticles (NPs) via the coprecipitation method. B) Required overpotentials to achieve 10 mA cm^{-2}. C) Tafel plots with the corresponding Tafel slopes for the OER process. Reproduced from Ref. [65] with permission. Copyright 2017, American Chemical Society. HER performance of the mp-FeS_2 in alkaline media (pH 13). D) Polarization curves and E) Tafel plots of the commercial FeS_2, mp-FeS_2, 20% Pt/C, and the bare Ni foam in 0.1 M KOH at a scan rate of 10 mV s^{-1}. Reproduced from Ref. [69] with permission. Copyright 2017, American Chemical Society. F) SEM image (insets: shell thickness distribution of hollow spheres (FeNCS-1000) and scheme of a hollow graphitic sphere), and simultaneously acquired. G) TEM image of FeNCS-1000 and TEM image of a single Fe-free N-doped hollow carbon spheres (NHCS) particle for comparison. H, I) Performance testing in O_2-saturated 0.1 M KOH solution. Rotating disk electrode voltammograms (rotation speed: 1600 rpm; scan rate: 10 mV s^{-1}; ring potential: 0.2 V) and the calculated peroxide yields. Reproduced from Ref. [70] with permission. Copyright 2017, Royal Society of Chemistry.

promoting the mass/charge transport as well as improving the accessibility to the Fe–N_2 sites active sites.

Moreover, metal chalcogenides containing nonprecious transition metal nanomaterials are regarded as a promising electrocatalyst for applications of efficient water splitting. Miao *et al.*[69] prepared mp-FeS_2 NPs with a high surface area (128 $m^2 g^{-1}$) by sol-gel method for highly efficient electrocatalytic HER. The high surface-area mp-FeS_2 NPs showed an outstanding HER activity delivering a current density of 10 mA cm^{-2} at a low overpotential of 96 mV, a small Tafel slope of 78 mV dec^{-2} and maintained the initial current density for 24 h at a constant overpotential of 100 mV (Figure 3D, E). Furthermore, the DFT results confirmed that the high catalytic performance of mp-FeS_2 for HER and low in the activation barrier was due to an abundance of (210) surface in mp-FeS_2. Zhou *et al.*[70] prepared macroporous core-graphitic mp-shell Fe–N-doped carbon spheres (FeNCSs) by using *in situ* template approach for ORR electrocatalysis. The shell thickness of mp-shell Fe–N can be clearly observed from TEM images, as shown in Figure 3F. Owing to unique structural properties that are contributed by the synergy of Fe–N_x-coordinated moieties, the as-prepared FeNCS showed an excellent ORR activity, including a $E_{1/2}$ of 0.886 V, which is 15 mV more positive than that of commercial Pt/C catalysts; stability; and outstanding tolerance to the methanol crossover compared to benchmark Pt/C catalysts in both acidic and alkaline electrolytes (Figure 3G, H).

Benefiting from the high specific surface area, permanent porosity, three-dimensional (3D) structure, as well as the diversity in organic and metal centers, MOFs have aroused great interest in the field of EC.[71] MOFs are suitable precursors for the fabrication of various electrocatalysts such as metal, or metal oxide, and heteroatom-doped containing carbon material by pyrolysis.[72] It is important to develop the single-atom catalyst, which provides efficient active sites with hierarchical pores for mass transfer and easily accessible active sites through rational design of MOFs to improve the electrocatalytic performance. Fe-based MOF with iron active configuration showed excellent electrocatalytic performance for various applications. Table 3 summarized typical MOF-derived iron containing-mesoporous structures for electrochemical water splitting.

Table 4. Summary of the electrochemical performance mp-FeNSs for LiBs.

Materials	Electrochemical performance			Ref.
	Current density [mA g^{-1}]	Cycle number	Capacity retention [mAh g^{-1}]	
Fe_2VO_4/nitrogen-doped carbon	500	250	1002	[107]
Fe_2O_3	100	200	1460	[108]
Cobalt/iron oxide (CFO)	500	250	635	[109]
$NiFe_2O_4$	100	150	1105.3	[110]
Fe_2O_3	400	300	2000	[111]
CN@Fe_3O_4@ CN	100	300	1048	[112]
Fe_3O_4@N-HPCNs	100	100	1240	[113]

4. Energy Storage Using mp-FeNSs

Next-generation energy storage technology demands high energy density, simple fabrication procedure, better security, faster recharge, and lower cost and earth-abundant materials. As a result, various energy storage devices have been developed, including sodium ion batteries, Zn-air batteries,[90] LiB,[91] many other rechargeable batteries,[92] and SCs.[93] Among these energy storage devices LiBs have become most widely used for medical microelectrodes, portable devices, and electric vehicles due to one of the outstanding characteristics having high energy density. The performance of LiB is mainly dependent on the specific capacitance. Practically, gravimetric, volumetric, and areal capacities are used to describe the lithium storage capacity per unit mass, volume, and area, respectively.[94] Similarly, the performance of SC is mainly dependent on the energy density, specific capacitance, cycling stability, rate capability, and power density.[95] The electrochemical performance of mp-FeNSs based materials for LiBs and SCs are shown in Table 4 and Table 5, respectively.

The special features of nanomaterials, including their high surface area, and altered physical and chemical properties, makes them highly preferred for the energy sector applications such as rechargeable batteries and SCs. LiBs and SCs are the key research areas expected to provide solutions to the complex energy storage gridlock. Applications of mp-FeNSs for large scale ECS systems have drawn tremendous attention. Their applications especially in SC and rechargeable LiBs are

Table 3. Summary of a recent Fe-based MOF for electrochemical water splitting.

Catalyst	Preparation method	Application	Electrolyte	Performance	Ref.
Fe-N-S-CNT	pyrolysis of zeolitic imidazolate frameworks (ZIF)-8 impregnated with iron salt	ORR	0.1 M KOH 0.5 M H_2SO_4	$E_{1/2}$ = 0.91 V $E_{1/2}$ = 0.85 V	[81]
Fe-N/C	host-guest chemistry	ORR	0.5 M H_2SO_4	$E_{1/2}$ = 0.735 V	[82]
Fe-ZIF	chemical doping of Fe ions into ZIF networks followed by one-step thermal activation	ORR	0.5 M H_2SO_4	$E_{1/2}$ = 0.85 V	[83]
Fe-N/C	cage-confinement synthesis strategy	ORR	0.1 M KOH	$E_{1/2}$ = 0.85 V	[84]
FeCo-NC nanofibers	electrospun	ORR OER	0.1 M KOH	$E_{1/2}$ = 0.869 V η^{10} = 1.686 V	[85]
Fe-Ni@nanocube-CNTs	pyrolysis of a bimetallic MOF	OER HER	1 M KOH	η^{10} = 0.274 V η^{10} = 0.202 V	[71]
Fe(III) dicarboxlyalte framework	host/guest geometries and modular synthesis strategy	OER	Alkaline water at pH = 13	η^{10} = 0.225 V	[86]
Fe/$Ni_{2.4}$/$Mn_{0.4}$	solvothermal synthesis	OER	1 M KOH	η^{20} = 0.236 V	[87]
NC@Fe_3O_4	pyrolysis ofpolyaniline(PANI)-coated Fe-based MO	ORR	0.1 M KOH	E_{onset} = 0.058 V	[88]
Fe/Ni-MOFs/N-graphene	solvent thermal	ORR	0.1 M KOH	E_{onset} = 1.09 V	[89]

Table 5. Performance mp-FeNSs based electrodes in supercapacitors.

Materials	Specific capacitance@ current density	Cycling stability	Ref.
$LaFeO_3$	241.3 $F g^{-1}$ at 1 $A g^{-1}$	92.2% @5000 cycles	[114]
FeOOH NFs@MWCNTs	345 $F g^{-1}$ at 1 $A g^{-1}$	76.4% @5000 cycles	[115]
$NiCoFeO_4$	1263 $F g^{-1}$ at 1 $A g^{-1}$	94%@4000 cycles	[116]
y-Fe_2O_3//MWCNTs/ PEDOT-PSS	65 $F g^{-1}$ at 2.4 $A g^{-1}$	94%@4000 cycles	[117]
The Fe_3O_4/PANI	1669.18 $F g^{-1}$ at 1 $A g^{-1}$	96.5% @25,000 cycles	[118]
$NiFe_2O_4$	584.63 $F g^{-1}$ at 0.5 $mA cm^{-2}$	91%@2000 cycles	[119]

gaining much attention due to their affordable cost, higher theoretical capacity, improved safety conditions, and non-toxicity.

4.1. mp-FeNSs for Lithium-Ion Batteries

Rechargeable LiBs have a long history of use in consumer electronics because of their high-power density and stability over a period of usage. The applications of LiBs in large scales like electric vehicles and electric power storage systems have been hampered by the limited availability of lithium resource in the world coupling with their low energy and power densities and safety issues. To satisfy the ever-increasing demand from this side, there is a need to search and improve the life cycle and energy density of LiBs. On the efforts of developing LiBs with higher capacity and efficient electrolyte, iron-based nanomaterials have been suggested to be a promising option to replace high cost lithium because of its abundance, higher theoretical storage capacity, lower cost, and safety.[96] Kong *et al.*[96a] synthesized a mp-electrode material of single-crystal from iron and cobalt through solvothermal method followed by calcination. To increase the activity of the electrode material, an element doping approach was employed. In this process, cobalt was utilized as a dopant (Co^{2+}) to further improve the conductivity of the synthesized material. After 200 cycles, the synthesized electrode material has demonstrated an enhanced reversible and cycling stabilities of (1222 $mA h g^{-1}$ and 200 $mA g^{-1}$ at 200 $mA g^{-1}$ and 500 $mA g^{-1}$ current densities, respectively) (Figure 4A–C).

Hundreds of unique Fe_2O_3 nanostructured materials, including NPs, NRs, nanotubes, nanoflakes, nanosheets, nanodiscs, nanowires, nanoflowers, and nanospindles, have been pertinently synthesized to improve the conductivity and cycle stability of the materials for ECS applications.[97] Additionally, various mp-Fe_2O_3 nanostructures have been synthesized because of their unique features in accommodating large strain and enhanced charge diffusion. Zhou *et al.*[98] synthesized mp-α-Fe_2O_3/cyclized-polyacrylonitrile (C-PAN) that has demonstrated superior power and energy density and cycling stability over graphite materials. To improve the electrical conductivity and enhance adhesion with active materials, C-PAN as coating material was employed instead of the common carbon additives. Compared to conventional graphite materials, this new material has demonstrated higher power density and retained capacity (reversible) of 996 $mAh g^{-1}$ after 100 cycles at 0.2 C. (Figure 4D, E).

Lithium metal orthosilicates are also of great interest in improving the application of LiBs in electric vehicle transportation. Previous studies have indicated that lithium metal orthosilicates can provide higher capacity of up to 330 $mA h g^{-1}$ which makes them potential options in LiB applications. The electrochemical performance of lithium metal orthosilicates is significantly influenced by the synthesis routes.[96b] Multiple lithium iron silicate synthesis routes have been reported, including solution and solid-state synthesis methods, with their pros and cons. So far, lithium metal orthosilicates syntheses have been based on the application of iron (II) salts as a precursor. This synthesis process was complicated due to the annealing process that requires higher temperature. To simplify the synthesis route and the reduction production cost of applying (Fe (II)) salt as the precursor, Wei *et al.*[96b] produced a mp-C-coated nanostructured lithium iron silicate based on Fe (III) salts with comparable capacity and stability to those derived from Fe(II) salts through a facile method. The process involves precipitation of ethylenediamine intermediate hydrothermally followed by the formation of crystalline Li_2FeSiO_4 through annealing with diluted H_2 gas. The application of ethylenediamine in the synthesis process helps the formation of the Fe^{3+} silicate complex (hydrated), which facilitates the crystallization of nanostructured lithium iron silicate.

Iron fluoride is one of the Fe-based nanomaterials with high operation voltage, large theoretical capacity, plentiful sources, and better safety with potential application in LiBs.[99] Despite its advantages, iron fluoride suffers from poor electrochemical performances limiting its applications in LiBs. Various techniques have been used to improve the conductivity of the iron fluoride including the introduction of conductive materials like mp-carbon, carbon nanotubes, carbon nanohorns and graphite oxide. Although the rate capacity of the iron fluoride is increased, these techniques are poor in increasing the overall capacity of the cathode material due to the presence of inactive agents. Another approach is the synthesis of iron fluoride-based nanostructures such as nanospheres, nanowires, and hollow microspheres to improve the rate performance of the battery. According to Han *et al.*[99] iron fluorides with hierarchical structures show better performance compared to other structures because of their large specific surface area. A low-cost monodispersed hierarchical mp-iron fluoride was prepared using iron (III) acetylacetonate as iron source through a reverse micelle method. The iron fluoride-based nanomaterial has an exchange rate capability around 255.3 $mAh g^{-1}$ at 100 $mA g^{-1}$ and 143.2 $mAh g^{-1}$ after at 1000 $mA g^{-1}$. The prolonged cycling reversibility coupled with higher performance makes it preferable for LiBs applications. Different investigations were undergone to improve the limitations of iron trifluoride (FeF_3) including the strong ionic bond in Fe—F. Different options have been sought, such as structural change and/or coating with conducting species like carbon metal fluoride nanocomposites, FeF_3/C, FeF_3/carbon nanotube, FeF_3/

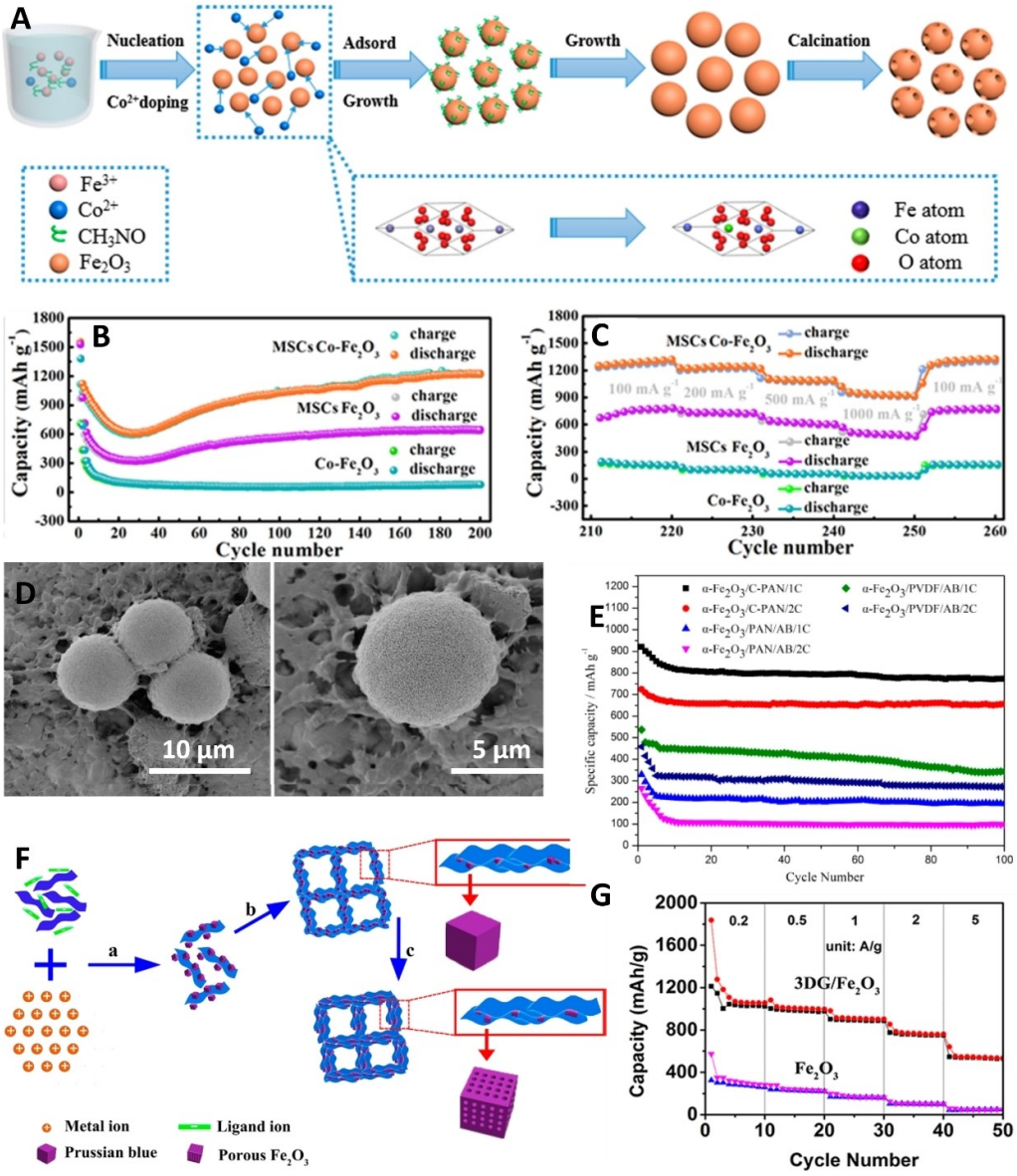

Figure 4. Fe-based mp-electrodes for LiB. A) Schematic of the proposed formation mechanism of mp-single crystals Co-Fe_2O_3. B) Charge – discharge profiles at a current density of 200 mA g^{-1}. C) Rate capability at a current density ranging from 100 to 1000 mA g^{-1}. Reproduced from Ref. [96a] with permission. Copyright 2017, American Chemical Society. D) SEM images of α-Fe_2O_3 (a,b,c) and α-Fe_2O_3/cyclized-polyacrylonitrile (C-PAN) composite. E) Cycling performances of α-Fe_2O_3/C-PAN, α-Fe_2O_3/PAN/acetylene black (AB), and α-Fe_2O_3/polyvinylidene fluoride) PVDF)/AB composites at large current densities of 1 C and 2 C for 100 cycles. Reproduced from Ref. [98] with permission. Copyright 2016, American Chemical Society. F) Schematic of the preparation procedure of three-dimensional graphene (3DG)/Fe_2O_3 G) Rate performance of 3DG/Fe_2O_3 and Fe_2O_3. Reproduced from Ref. [96c] with permission. Copyright 2017, American Chemical Society.

polystyrene sulfonate, FeF_3/ordered mp-carbon, FeF_3/graphene, and FeF_3/nickel ammine nitrate with improved performances. The other limitation of FeF_3 as a cathode material was the dense crystalline structure, which influences its performance. As alternatives to the crystalline structure, the expanded structures were carefully designed via water-stabilized ion transport channels. Previously employed preparation mechanisms of $FeF_3 \cdot 0.33H_2O$ materials suffer from poor reproducibility, expensive production cost, and safety issues, which hinder their large-scale application. To overcome these challenges, Zhai *et al.*[100] synthesized hierarchical micro/nanostructured $FeF_3 \cdot 0.33H_2O$ materials using a mild solvothermal strategy. The process involved the adjustment of the solvent/temperature to synthesize the desired iron fluoride materials with a unique hierarchical morphology. Lowering the reaction temperature to 150 °C has dehydrated $FeF_3 \cdot 3H_2O$ into micro/nanostructured $FeF_3 \cdot 0.33H_2O$, that provides enough reaction sites. Compared to the bulk $FeF_3 \cdot 0.33H_2O$, which is traditionally prepared by heat treatment, the newly prepared nanostructured $FeF_3 \cdot 0.33H_2O$ has demonstrated improvement in the stability and rate capability. The integration of metal oxides with conductive materials like graphene can have the potential to improve the electronic transport in LiBs due to the relative stability and higher electrical conductivity of the materials. In

their work, Jiang *et al.*[96c] implemented encapsulation of porous Fe_2O_3 nano-frameworks into graphene skeleton with improved structural stability and charge transport during electrochemical reactions. In its first cycles of 130, the electrode material delivered a capacity of 1129 $mA\,h\,g^{-1}$ at 0.2 Ag^{-1} and retaining the stability even after 1200 cycles at 5 $A\,g^{-1}$ (Figure 4F, G).

TMO nanostructures mixed with inorganic and organic composites have attracted the researcher's attention because of their excellent electrochemical performance. The organic-inorganic hybrids of mp-FeNSs have been synthesized for different applications, including those for catalysts and adsorbents. Iron phosphate mp-FeNS is one of the promising candidates for LiB applications. So far, different mechanisms have been employed to prepare and optimize the practical application of organic-inorganic hybrid mp-FeNSs in different sectors. However, most of them could not demonstrate the practical utility of the prepared material. The prepared organosilica mp-FeNSs suffer from amorphous structure of the pore walls, high cost, and limited reaction conditions that challenged its applications in a wide range of chemical fields. Pramanik *et al.*[91] synthesized an organic-inorganic nonsilica-based hybrid iron phosphonate material with comparable stability and enhanced surface area. The preparation process involved a pore wall formation using nitrilotris (methylene) triphosphonic acid and iron nitrate, while structure-directing agent using cetyltrimethylammonium bromide. The obtained mp-iron phosphonate materials demonstrated higher retention capacity with very good cycling stability.

4.2. mp-FeNSs Electrodes for Supercapacitors

Supercapacitors (SCs) have drawn remarkable interest because of their fast charging/discharging value ($>$100,000 cycles), over 10, 000 $W\,Kg^{-1}$ of power density and less resistance and extensive cycle life.[101] An intermediate between conventional capacitors and rechargeable batteries,[102] SCs are composed of a separator preventing contact between electrodes, electrodes (anode and cathode), and an electrolyte that facilitates movement of ions. Among components, electrodes play most important part in determining performance of SCs.[103] The applications of mp-FeNSs in SCs have been thoroughly explored due to their prominent supercapacitive property, and abundant non-toxic elements.

Currently, developments in SC manufacturing technology have increased the capacity and power density of the materials. Kore *et al.*[101a] synthesized Fe_2O_3 based mp-NPs electrode material using $Fe(NO_3)_3\cdot 9H_2O$ and NH_4HCO_3 precursors through a robust solvent-deficient route, that demonstrated improved capacitive performance. A difference was observed between untreated and rinsed precursors. The rinsed mp-Fe_2O_3 NPs have a higher energy density, surface area, and enhanced power density than untreated ones. Moreover, after 2000 cycles both the untreated and treated Fe_2O_3 have maintained their stability up to 78% and 84%, respectively. Progress has been made in solving the challenging aspects of SCs, especially those based on iron oxide materials, as they are poor in electrical conductivity. Studies have indicated that dropping a metal oxide on another metal oxide that has different electrochemical and morphological features can improve the electrochemical performance of SCs.[13b] Maitra *et al.*[101b] produced a supercapacitor electrode material with higher performance through combinations of polypyrrole, iron oxide, and vanadium oxide hydrate. The process involved decoration of the as-synthesized cobalt vanadium hydrate using iron oxide nanospheres. The electrode demonstrated 1202 $F\,g^{-1}$ specific capacitance, 38.2 $W\,h\,kg^{-1}$ energy density and 95% of cyclic stability. Furthermore, mp-Fe_2O_3 NPs under the robust process of solvent-deficient synthesis showed 469 $F\,g^{-}$ of specific capacitance and remained 84% of this value after 2,000 cycles.

The other developmental progress in SCs is the application of inexpensive and environmentally safe iron oxide as a negative electrode material synthesis. So far, negative electrode materials were based on carbon materials in alkaline electrolytes. These would have been attributed to the low capacitance of carbon-based. Despite the advantages of iron oxide over carbon material as an electrode in SCs, the preparation mechanism has challenged the application of iron oxide. So far, different techniques have been employed to improve application of iron oxide in the SCs, most of them have been unable to produce the desired specific capacity. To overcome the challenges, Mohamed *et al.*[104] synthesized mp-Fe_3O_4 film through a facile way that involved an *in situ* hydrothermal process as a negative electrode for SC application. The process improved the stability and capacity of the synthesized Fe_3O_4 film, with an enhanced specific surface area of 247 $m^2\,g^{-1}$ and maintained a capacity of 221 $C\,g^{-1}$ and 154 $C\,g^{-1}$ over a wider range of current densities of 1 $A\,g^{-1}$ and 50 $A\,g^{-1}$, respectively. The applications of iron-based materials in SCs are emerging as potential options because of their relatively superior electrochemical properties as compared to electric-double layer capacitors.

Iron-based supercapacitors suffer from a low rate of diffusion and poor electrical conductivities that hampered their wide applications. Sahoo *et al.*[105] have synthesized a 3D nanoarchitecture of Fe–Ni–Co oxide nanoflake arrays on Ni, which demonstrated an outstanding capacitance. The as-prepared SC electrode showed 867 $F\,g^{-1}$ of capacitance and 92.3% of retention stability after 10,000 cycles of charge-discharges. Mohamed *et al.*[106] also reported that mixing different TMO like cobaltite ($NiCo_2O_4$) and iron cobaltite ($FeCo_2O_4$) can enhance the activity of the resulting porous nonmaterial. In this study, the obtained crystalline $FeCo_2O_4$ nanosheet have demonstrated 853.8 $F\,g^{-1}$ of specific capacitance and 87.5% (after 3,00 cycles) cycling stability (Figure 5A, B).

Prominent achievements regarding improvement in the energy density of SCs without affecting power density was reached in recent years. Several techniques were employed to boost the energy density, such as asymmetric SCs that are composed of two different electrodes both as power and energy sources. However, such asymmetric SCs suffer from large capacitance mismatch between the anode and cathode due to the intrinsically low electric double-layer capacitance in carbon nanomaterials, resulting in low energy storage capacity

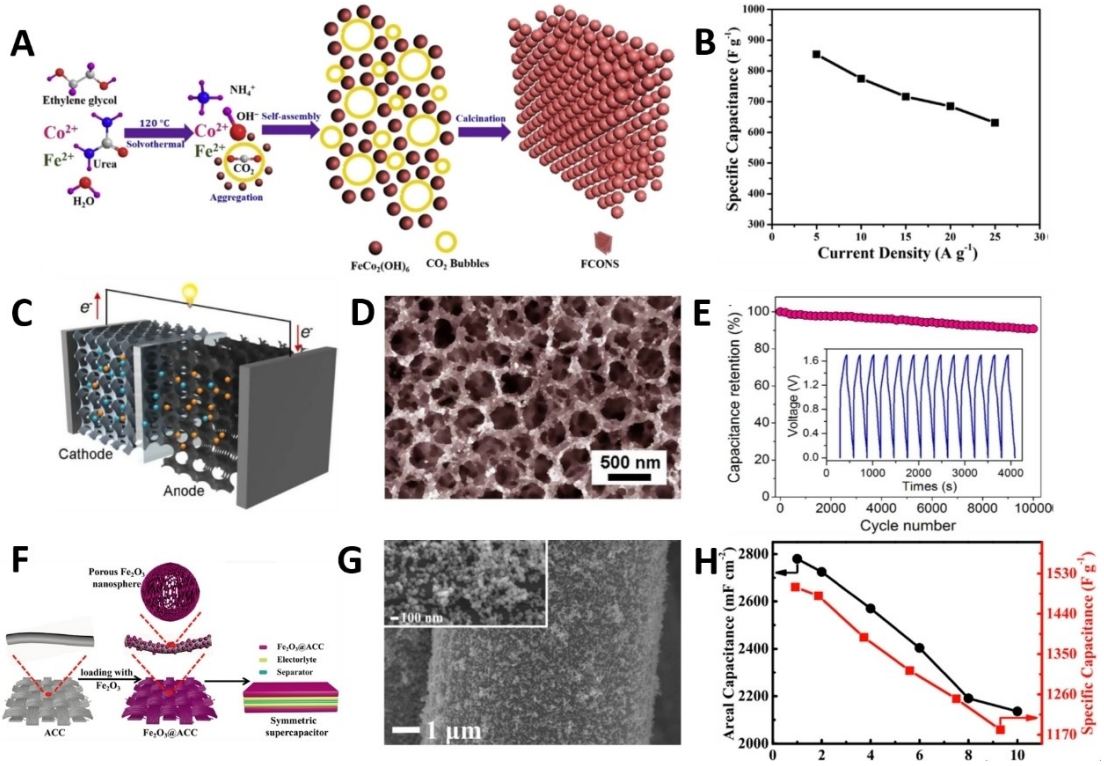

Figure 5. Fe-based mp-NSs for SCs: A) Schematic of the formation of $FeCo_2O_4$ nanosheet mp-structure. B) SC performance of $FeCo_2O_4$ nanosheet electrode in 6 M KOH electrolyte-specific capacitance vs. current density. Reproduced from Ref. [106] with permission. Copyright 2017, Elsevier. C) Schematic showing asymmetric SCs comprising of cathode and anode electrodes with 3D bicontinuous nanoporous architectures. D) SEM image of 3D NP nitrogen-doped graphene/iron oxide (NDG/FeO_x) hybrid materials. E) Capacitance retention vs. cycle number for the asymmetric SC (ASC) at a galvanostatic charge/discharge current densities of 9 A g^{-1}. Inset: Representative voltage-time profiles during the charge/discharge cycles. Reproduced from Ref. [93] with permission. Copyright 2017 Elsevier. F) Schematic of the Fe_2O_3@ACC electrode and the structure of symmetric SC. G) FESEM images of the Fe_2O_3 nanospheres on activated carbon cloth at different magnifications. H) Areal and specific capacitances of the Fe_2O_3@ACC electrode vs. current density. Reproduced from [97c] with permission. Copyright 2018 Elsevier.

of the capacitors. To enhance the performance rate and capacity of asymmetric SCs, it is mandatory to develop anode materials that have similar capacitance. Liu *et al.*[93] developed a 3D nanoporous high performing asymmetric SCs like nickel-iron battery from N-doped graphene/iron oxide. The as-synthesized anode material has 142 Wh kg^{-1} and 1.4 kW kg^{-1} of energy and power density, respectively (Figure 5C–E). Li *et al.* have enhanced the poor electrical conductivity and surface area of Fe_2O_3 by anchoring on activated carbon. The produced porous nanosphere has demonstrated 9.2 mW h cm^{-3} and 12 mW cm^{-3} energy and power densities making them a potential candidate for SCs (Figure 5F–H).

5. Conclusion and Perspectives

We have shown the recent advances in Fe-based mesoporous nanostructures (mp-FeNSs) for electrochemical water splitting, Li-ion batteries (LiBs), and supercapacitors (SCs) for energy conversion and storage (ECS). The physical and chemical uniqueness, synthesis techniques, and the mechanism of electrochemical water splitting of mp-FeNSs were discussed. Then, different mp-FeNSs that could enhance the electrochemical reaction for ECS were highlighted. It is shown that porous materials with different pore sizes and large surface areas are effective for ECS applications. These unique structural advantages afford mp-structures an extraordinary enhanced electrochemical reaction. mp-FeNSs have localized *d*-electrons within the walls between that pores are endowed with unusual magnetic, optical, electrical, and semiconducting properties. Furthermore, Fe is the principal active center in nanocomposites used for ECS applications. Despite significant reports on mp-FeNSs performance in energy applications recently, the researchers in the field may face challenges. The following aspect could be considered in the future development of highly efficient mp-FeNSs based electrodes.

At present, most of the synthesis approaches are complicated and so cost-ineffective, which is inappropriate for industrial applications. A new approach for the synthesis and design of the electrode are expected. Experimental and theoretical methods are needed to rationalize and resolve the synthesis design and electrode fabrication for commercial applications.

The low intrinsic electrical conductivity of Fe-based nanostructure is one of the challenges in electrocatalysis. It is crucial to understand and perform how to improve the undesirable electrochemical and cycling performance of mp-FeNSs caused by poor conductivity for fabricating electrodes of ECS. The

catalytic activity of these nanostructures can be enhanced by choosing an appropriate dopant that can improve the electrical conductivity and accurately regulate their morphology.

Some fundamental mechanisms of the mp-FeNSs based electrodes in aqueous electrolyte remain unanswered, particularly regarding the charge and electron transfer during the electrochemical interface reactions. We believe that understanding some basic mechanism could offer a direction for the structural design of mp-FeNSs based electrodes.

Various advanced *in situ* electrochemical spectroscopy/microscopy (AFM, XRD, TEM, SEM, XPS) must be used to monitor the electrochemical mechanism of electrode materials. The study of the reaction mechanism using these advanced instruments could guide the synthesis and design of new mp-FeNSs for ECS.

Acknowledgements

This work was supported by grants from Korea Hydro & Nuclear Power Co. Ltd. (No. 2018-RFP-Tech-21) and National Research Foundation of Korea (NRF-2019R1 A2 C2007825, 2017R1 A4 A1015627). The sponsors played no role in the writing of this review paper and in the decision to submit the article for publication.

Conflict of Interest

The authors declare no conflict of interest.

Keywords: electrochemical water splitting · Fe-based nanostructures · Li-ion battery · mesoporous · supercapacitor

[1] P. Poizot, F. Dolhem, *Energy Environ. Sci.* **2011**, *4*, 2003–2019.
[2] J. Wang, W. Cui, Q. Liu, Z. Xing, A. M. Asiri, X. Sun, *Adv. Mater.* **2016**, *28*, 215–230.
[3] P. Simon, Y. Gogotsi, B. Dunn, *Science* **2014**, *343*, 1210–1211.
[4] R. Schmuch, R. Wagner, G. Hörpel, T. Placke, M. Winter, *Nat. Energy* **2018**, *3*, 267.
[5] Q. An, F. Lv, Q. Liu, C. Han, K. Zhao, J. Sheng, Q. Wei, M. Yan, L. Mai, *Nano Lett.* **2014**, *14*, 6250–6256.
[6] S. Kandalkar, D. Dhawale, C.-K. Kim, C. Lokhande, *Synth. Met.* **2010**, *160*, 1299–1302.
[7] L. L. Zhang, R. Zhou, X. Zhao, *J. Mater. Chem.* **2010**, *20*, 5983–5992.
[8] W. Li, J. Liu, D. Zhao, *Nat. Rev. Mater.* **2016**, *1*, 16023.
[9] a) S. E. Moosavifard, S. K. Kaverlavani, J. Shamsi, A. Bakouei, *J. Mater. Chem. A* **2017**, *5*, 18429–18433; b) L. Yu, H. Hu, H. B. Wu, X. W. D. Lou, *Adv. Mater.* **2017**; c) B. Y. Guan, X. Y. Yu, H. B. Wu, X. W. D. Lou, *Adv. Mater.* **2017**; d) Y. Lu, L. Yu, M. Wu, Y. Wang, X. W. D. Lou, *Adv. Mater.* **2018**, *30*; e) L. Yu, J. F. Yang, B. Y. Guan, Y. Lu, X. W. D. Lou, *Angew. Chem.* **2018**, *130*, 178–182; *Angew. Chem. Int. Ed.* **2018**, *57*, 172–176.
[10] a) J. Wei, Z. Sun, W. Luo, Y. Li, A. A. Elzatahry, A. M. Al-Enizi, Y. Deng, D. Zhao, *J. Am. Chem. Soc.* **2017**, *139*, 1706–1713; b) W. Li, J. Liu, D. Zhao, *Nat. Rev. Mater.* **2016**, *1*, 16023; c) D. Liu, L. T. Tufa, J. Lee, *Electrochim. Acta* **2019**, *313*, 389–396.
[11] a) D. Luo, Y.-P. Deng, X. Wang, G. Li, J. Wu, J. Fu, W. Lei, R. Liang, Y. Liu, Y. Ding, *ACS Nano* **2017**, *11*, 11521–11530; b) C. C. H. Tran, J. Santos-Peña, C. Damas, *J. Phys. Chem. C* **2017**.
[12] Z. Yu, P. Zhang, Y. Feng, S. Li, Y. Pei, *J. Am. Chem. Soc.* **2016**, *99*, 2615–2624.
[13] a) S. Tanaka, Y. V. Kaneti, R. Bhattacharjee, M. N. Islam, R. Nakahata, N. Abdullah, S.-i. Yusa, N.-T. Nguyen, M. J. Shiddiky, Y. Yamauchi, *ACS Appl. Mater. Interfaces* **2017**, *10*, 1039–1049; b) L. T. Tufa, S. Oh, J. Kim, K.-J. Jeong, T. J. Park, H.-J. Kim, J. Lee, *Electrochim. Acta* **2018**, *290*, 369–377.
[14] A. W. Golubkov, D. Fuchs, J. Wagner, H. Wiltsche, C. Stangl, G. Fauler, G. Voitic, A. Thaler, V. Hacker, *RSC Adv.* **2014**, *4*, 3633–3642.
[15] I. G. Denisov, T. M. Makris, S. G. Sligar, I. Schlichting, *Chem. Rev.* **2005**, *105*, 2253–2278.
[16] V. R. Stamenkovic, D. Strmcnik, P. P. Lopes, N. M. Markovic, *Nat. Mater.* **2017**, *16*, 57.
[17] M. S. Burke, M. G. Kast, L. Trotochaud, A. M. Smith, S. W. Boettcher, *J. Am. Chem. Soc.* **2015**, *137*, 3638–3648.
[18] Z. Zhou, Q. Zhang, J. Sun, B. He, J. Guo, Q. Li, C. Li, L. Xie, Y. Yao, *ACS Nano* **2018**, *12*, 9333–9341.
[19] G.-L. Li, C.-D. Liu, S.-M. Chen, C. Hao, G.-C. Cheng, Y.-Y. Xie, *Inter. J. Hydrog. Energy* **2017**, *42*, 4133–4145.
[20] H. Bandal, K. K. Reddy, A. Chaugule, H. Kim, *J. Power Sources* **2018**, *395*, 106–127.
[21] J. Jin, W. A. Hines, C.-H. Kuo, D. M. Perry, A. S. Poyraz, Y. Xia, T. Zaidi, M.-P. Nieh, S. L. Suib, *Dalton Trans.* **2015**, *44*, 11943–11953.
[22] N. Zhang, X. Xiao, H. Pang, *Nanoscale Horiz.* **2019**, *4*, 99–116.
[23] V. Nithya, N. S. Arul, *J. Power Sources* **2016**, *327*, 297–318.
[24] K. G. Kottrup, S. D'Agostini, P. H. van Langevelde, M. A. Siegler, D. G. Hetterscheid, *ACS Catal.* **2018**, *8*, 1052–1061.
[25] a) Y. Kaneti, R. Salunkhe, N. L. W. Septiani, C. Young, X. Jiang, Y. He, Y. Kang, Y. Sugahara, Y. Yamauchi, *J. Mater. Chem. A* **2018**; b) X. Deng, K. Chen, H. Tüysüz, *Chem. Mater.* **2016**, *29*, 40–52.
[26] M. Inagaki, M. Toyoda, Y. Soneda, S. Tsujimura, T. Morishita, *Carbon* **2016**, *107*, 448–473.
[27] Z. Mai, J. Chen, Y. Hu, F. Liu, B. Fu, H. Zhang, X. Dong, W. Huang, W. Zhou, *J. Colloid Interface Sci.* **2017**, *508*, 184–195.
[28] C. Ciotonea, B. Dragoi, A. Ungureanu, C. Catrinescu, S. Petit, H. Alamdari, E. Marceau, E. Dumitriu, S. Royer, *Cat. Sci. Technol.* **2017**, *7*, 5448–5456.
[29] T. Sawada, T. Serizawa, *Bull. Chem. Soc. Jpn.* **2018**, 91, 455–466.
[30] L. Han, X. Luo, X. Luan, C. Wang, Y. Zhao, J. Lu, *Int. J. Hydrogen Energy* **2016**, *41*, 15783–15789.
[31] J.-j. Ban, G.-C. Xu, L. Zhang, H. Lin, Z.-p. Sun, Y. Lv, D.-Z. Jia, *J. Solid State Chem.* **2017**, *256*, 151–157.
[32] H. D. Follmann, O. N. Oliveira, D. Lazarin-Bidóia, C. V. Nakamura, X. Huang, T. Asefa, R. Silva, *Nanoscale* **2018**, 10, 1704–1715.
[33] S. Zhu, H. Tian, N. Wang, B. Chen, Y. Mai, X. Feng, *Small* **2018**, *14*, 1702755.
[34] S. Zhu, B. Dong, Y. Yu, L. Bu, J. Deng, S. Zhou, *Chem. Eng. J.* **2017**, *328*, 527–535.
[35] E. Lim, C. Jo, J. Lee, *Nanoscale* **2016**, *8*, 7827–7833.
[36] D. Maiti, S. Mukhopadhyay, P. S. Devi, *ACS Sustainable Chem. Eng.* **2017**, *5*, 11255–11267.
[37] M. Ma, F. Yan, M. Yao, Z. Wei, D. Zhou, H. Yao, H. Zheng, H. Chen, J. Shi, *ACS Appl. Mater. Interfaces* **2016**, *8*, 29986–29996.
[38] J. Wang, X. Shao, Q. Zhang, G. Tian, X. Ji, W. Bao, *J. Mol. Liq.* **2017**, *248*, 13–18.
[39] J. Xu, D. Xiong, I. Amorim, L. Liu, *ACS Applied Nano Materials* **2018**, *1*, 617–624.
[40] H. Wu, D. Lee, L. T. Tufa, J. Kim, J. Lee, *Chem. Mater.* **2019**, 31, 2263–2268.
[41] a) D. Sarkar, A. Shukla, D. Sarma, *ACS Energy Lett.* **2016**, *1*, 82–88; b) S. Yu, V. M. H. Ng, F. Wang, Z. Xiao, C. Li, L. B. Kong, W. Que, K. Zhou, *J. Mater. Chem. A* **2018**, *6*, 9332–9367.
[42] A. C. McKinlay, R. E. Morris, P. Horcajada, G. Férey, R. Gref, P. Couvreur, C. Serre, *Angew. Chem. Int. Ed.* **2010**, *49*, 6260–6266; *Angew. Chem.* **2010**, *122*, 6400–6406.
[43] J. Yang, Q. Zhang, Z. Wang, Z. Wang, L. Kang, M. Qi, M. Chen, W. Liu, W. Gong, W. Lu, *Adv. Energy Mater.* **2020**, *10*, 2001064.
[44] M. H. Yap, K. L. Fow, G. Z. Chen, *Green Energy Environ.* **2017**, *2*, 218–245.
[45] Y. Chen, S. Ji, S. Zhao, W. Chen, J. Dong, W.-C. Cheong, R. Shen, X. Wen, L. Zheng, A. I. Rykov, *Nat. Commun.* **2018**, *9*, 5422.
[46] J. Su, R. Ge, Y. Dong, F. Hao, L. Chen, *J. Mater. Chem. A* **2018**, *6*, 14025–14042.
[47] V. Tran, D. Lee, J. Kim, J. Lee, L. Tufa, C. Kim, J. Lee, *Nanoscale* **2020**, 12, 8453–8465.
[48] S. F. Hung, Y. Y. Hsu, C. J. Chang, C. S. Hsu, N. T. Suen, T. S. Chan, H. M. Chen, *Adv. Energy Mater.* **2018**, *8*, 1701686.

[49] M. Görlin, J. Ferreira de Araújo, H. Schmies, D. Bernsmeier, S. R. Dresp, M. Gliech, Z. Jusys, P. Chernev, R. Kraehnert, H. Dau, *J. Am. Chem. Soc.* **2017**, *139*, 2070–2082.
[50] J. Y. Chen, L. Dang, H. Liang, W. Bi, J. B. Gerken, S. Jin, E. E. Alp, S. S. Stahl, *J. Am. Chem. Soc.* **2015**, *137*, 15090–15093.
[51] A. M. Bruck, C. A. Cama, C. N. Gannett, A. C. Marschilok, E. S. Takeuchi, K. J. Takeuchi, *Inorg. Chem. Front.* **2016**, *3*, 26–40.
[52] Y. Chen, S. Ji, Y. Wang, J. Dong, W. Chen, Z. Li, R. Shen, L. Zheng, Z. Zhuang, D. Wang, *Angew. Chem. Int. Ed.* **2017**, *56*, 6937–6941; *Angew. Chem.* **2017**, *129*, 7041–7045.
[53] L. Jiao, G. Wan, R. Zhang, H. Zhou, S. H. Yu, H. L. Jiang, *Angew. Chem. Int. Ed.* **2018**, *57*, 8525–8529; *Angew. Chem.* **2018**, *130*, 8661–8665.
[54] L. Xie, R. Zhang, L. Cui, D. Liu, S. Hao, Y. Ma, G. Du, A. M. Asiri, X. Sun, *Ang. Chem.* **2017**, *129*, 1084–1088.
[55] a) N.-T. Suen, S.-F. Hung, Q. Quan, N. Zhang, Y.-J. Xu, H. M. Chen, *Chem. Soc. Rev.* **2017**, *46*, 337–365; b) T. Reier, H. N. Nong, D. Teschner, R. Schlögl, P. Strasser, *Adv. Energy Mater.* **2017**, 7,1601275 c) V. Vij, S. Sultan, A. M. Harzandi, A. Meena, J. N. Tiwari, W.-G. Lee, T. Yoon, K. S. Kim, *ACS Catal.* **2017**, *7*, 7196–7225; d) J. Durst, A. Siebel, C. Simon, F. Hasche, J. Herranz, H. Gasteiger, *Energy Environ. Sci.* **2014**, *7*, 2255–2260.
[56] M. Q. Yang, J. Wang, H. Wu, G. W. Ho, *Small* **2018**, *14*, 1703323.
[57] L. T. Tufa, K.-J. Jeong, V. T. Tran, J. Lee, *ACS Appl. Mater. Interfaces* **2020**, *12*, 6598–6606.
[58] A. M. Appel, M. L. Helm *ACS Catal.* **2014**, 4,630-633.
[59] S. Anantharaj, S. R. Ede, K. Sakthikumar, K. Karthick, S. Mishra, S. Kundu, *ACS Catal.* **2016**, *6*, 8069–8097.
[60] L. Han, S. Dong, E. Wang, *Adv. Mater.* **2016**, *28*, 9266–9291.
[61] B. K. Kang, M. H. Woo, J. Lee, Y. H. Song, Z. Wang, Y. Guo, Y. Yamauchi, J. H. Kim, B. Lim, D. H. Yoon, *J. Mater. Chem. A* **2017**, *5*, 4320–4324.
[62] K. Yan, Y. Lu, W. Jin, *ACS Sustainable Chem. Eng.* **2016**, *4*, 5398–5403.
[63] Z. Wu, X. Wang, J. Huang, F. Gao, *J. Mater. Chem. A* **2018**, *6*, 167–178.
[64] M.-S. Park, J. Kim, K. J. Kim, J.-W. Lee, J. H. Kim, Y. Yamauchi, *Phys. Chem. Chem. Phys.* **2015**, *17*, 30963–30977.
[65] A. Kumar, S. Bhattacharyya, *ACS Appl. Mater. Interfaces* **2017**, *9*, 41906–41915.
[66] X. Gao, X. Li, Q. Wang, C. You, X. Tian, C. Wang, Y. Hua, S. Liao, *J. Mater. Chem. A* **2020**, *8*, 2439–2444.
[67] X. Hong, Y. Xu, R. Wang, P. Du, Z. Zhao, K. Huang, H. Tang, Y. Liu, M. Lei, H. Wu, *Adv. Mater. Interfaces* **2020**, 2000740.
[68] T. Sun, P. Zhang, W. Chen, K. Wang, X. Fu, T. Zheng, J. Jiang, *Chem. Commun.* **2020**, *56*, 798–801.
[69] R. Miao, B. Dutta, S. Sahoo, J. He, W. Zhong, S. A. Cetegen, T. Jiang, S. P. Alpay, S. L. Suib, *J. Am. Chem. Soc.* **2017**, *139*, 13604–13607.
[70] T. Zhou, Y. Zhou, R. Ma, Q. Liu, Y. Zhu, J. Wang, *J. Mater. Chem. A* **2017**, *5*, 12243–12251.
[71] X. Zhao, P. Pachfule, S. Li, J. R. J. Simke, J. Schmidt, A. Thomas, *Angew. Chem. Int. Ed.* **2018**, *57*, 8921–8926; *Angew. Chem.* **2018**, *130*, 9059–9064.
[72] K. Jayaramulu, J. Masa, O. Tomanec, D. Peeters, V. Ranc, A. Schneemann, R. Zboril, W. Schuhmann, R. A. Fischer, *Adv. Funct. Mater.* **2017**, *27*, 1700451.
[73] L. He, B. Cui, B. Hu, J. Liu, K. Tian, M. Wang, Y. Song, S. Fang, Z. Zhang, Q. Jia, *ACS Appl. Mater. Interfaces* **2018**, *1*, 3915–3928.
[74] G. Liu, K. Wang, X. Gao, D. He, J. Li, *Electrochim. Acta* **2016**, *211*, 871–878.
[75] M. Yao, N. Wang, W. Hu, S. Komarneni, *Appl Catal. B: Environ.* **2018**, *233*, 226–233.
[76] G. Liu, X. Gao, K. Wang, D. He, J. Li, *Int. J. Hydrogen Energy* **2016**, *41*, 17976–17986.
[77] Q. Zhang, Y. Fan, W. Wang, N. Liu, J. Guan, *ChemElectroChem* **2020**, *7*, 118–123.
[78] M. Hafezi Kahnamouei, S. Shahrokhian, *ACS Appl. Mater. Interfaces* **2020**, *12*, 16250–16263.
[79] W. Chen, G. Qian, Q. Xu, C. Yu, M. Yu, Y. Xia, S. Yin, *Nanoscale* **2020**, *12*, 7116–7123.
[80] K. Zhan, C. Feng, X. Feng, D. Zhao, S. Yue, Y. Li, Q. Jiao, H. Li, Y. Zhao, *ACS Sustain.Chem. Eng.* **2020**, 8, 6273–6281.
[81] H. Jin, H. Zhou, D. He, Z. Wang, Q. Wu, Q. Liang, S. Liu, S. Mu, *Appl. Cat. B: Environ.* **2019**, *250*, 143–149.
[82] Q. Lai, L. Zheng, Y. Liang, J. He, J. Zhao, J. Chen, *ACS Catal.* **2017**, *7*, 1655–1663.
[83] H. Zhang, S. Hwang, M. Wang, Z. Feng, S. Karakalos, L. Luo, Z. Qiao, X. Xie, C. Wang, D. Su, *J. Am. Chem. Soc.* **2017**, *139*, 14143–14149.
[84] G. Ye, Q. He, S. Liu, Z. Kuangmin, Y. Su, W. Zhu, R. Huang, Z. He, *J. Mater. Chem. A* **2019**, 7,16508-15.
[85] L. Yang, S. Feng, G. Xu, B. Wei, L. Zhang, *ACS Sustainable Chem. Eng.* **2019**, *7*, 5462–5475.
[86] J.-Q. Shen, P.-Q. Liao, D.-D. Zhou, C.-T. He, J.-X. Wu, W.-X. Zhang, J.-P. Zhang, X.-M. Chen, *J. Am. Chem. Soc.* **2017**, *139*, 1778–1781.
[87] F. L. Li, Q. Shao, X. Huang, J. P. Lang, *Angew. Chem. Int. Ed.* **2018**, *57*, 1888–1892; *Angew. Chem.* **2018**, *130*, 1906–1910.
[88] S. Gao, B. Fan, R. Feng, C. Ye, X. Wei, J. Liu, X. Bu, *Nano Energy* **2017**, *40*, 462–470.
[89] X. Qin, Y. Huang, K. Wang, T. Xu, Y. Wang, M. Wang, M. Zhao, Q. Gao, *Ind. Eng. Chem. Res.* **2019**, 58, 10224–10237.
[90] K. Wu, L. Zhang, Y. Yuan, L. Zhong, Z. Chen, X. Chi, H. Lu, Z. Chen, R. Zou, T. Li, *Adv. Mater.* **2020**, *32*, 2002292.
[91] M. Pramanik, Y. Tsujimoto, V. Malgras, S. X. Dou, J. H. Kim, Y. Yamauchi, *Chem. Mater.* **2015**, *27*, 1082–1089.
[92] Y. Zhang, L. Tao, C. Xie, D. Wang, Y. Zou, R. Chen, Y. Wang, C. Jia, S. Wang, *Adv. Mater.* **2020**, *32*, 1905923.
[93] B.-T. Liu, M. Zhao, L.-P. Han, X.-Y. Lang, Z. Wen, Q. Jiang, *Chem. Eng. J.* **2018**, *335*, 467–474.
[94] F. Zhang, L. Qi, *Adv. Sci.* **2016**, *3*, 1600049.
[95] S. Pappu, K. Nanaji, S. Mandati, T. N. Rao, S. K. Martha, S. V. Bulusu, *Batteries & Supercaps* **2020**.
[96] a) H. Kong, C. Lv, C. Yan, G. Chen, *Inorg. Chem.* **2017**, *56*, 7642–7649; b) H. Wei, X. Lu, H.-C. Chiu, B. Wei, R. Gauvin, Z. Arthur, V. Emond, D.-T. Jiang, K. Zaghib, G. P. Demopoulos, *ACS Sustainable Chem. Eng.* **2018**, *6*, 7458–7467; c) T. Jiang, F. Bu, X. Feng, I. Shakir, G. Hao, Y. Xu, *ACS Nano* **2017**, *11*, 5140–5147.
[97] a) J. Zhang, J. Wan, J. Wang, H. Ren, R. Yu, L. Gu, Y. Liu, S. Feng, D. Wang, *Angew. Chem. Int. Ed.* **2019**, *58*, 5266–5271; b) Q. Hou, Q. Man, P. Liu, R. Jin, Y. Cui, G. Li, S. Gao, *Electrochim. Acta* **2019**, *296*, 438–449; c) J. Li, Y. Wang, W. Xu, Y. Wang, B. Zhang, S. Luo, X. Zhou, C. Zhang, X. Gu, C. Hu, *Nano Energy* **2019**, *57*, 379–387; d) S.-K. Park, G. D. Park, Y. C. Kang, *Nanoscale* **2018**, *10*, 11150–11157; e) J. Zhao, Z. Li, X. Yuan, Z. Yang, M. Zhang, A. Meng, Q. Li, *Adv. Energy Mater.* **2018**, *8*, 1702787; f) C. Zeng, W. Weng, T. Lv, W. Xiao, *ACS Appl. Mater. Interfaces* **2018**, *10*, 30470–30478; g) Z.-S. Zhu, J. Qu, S.-M. Hao, S. Han, K.-L. Jia, Z.-Z. Yu, *ACS Appl. Mater. Interfaces* **2018**, *10*, 30670–30679; h) S. Lee, H. Kim, H. M. Jung, *J. Electroanal. Chem.* **2016**, *770*, 44–49; i) Z. Wang, Z. Zhang, J. Xia, W. Wang, S. Sun, L. Liu, H. Yang, *J.Alloy Comp* **2018**, *769*, 969–976; j) Q. Du, Q. Gao, *Mater. Technol.* **2017**, *32*, 724–728.
[98] D. Wang, H. Dong, H. Zhang, Y. Zhang, Y. Xu, C. Zhao, Y. Sun, N. Zhou, *ACS Appl. Mater. Interfaces* **2016**, *8*, 19524–19532.
[99] Y. Han, H. Li, J. Li, H. Si, W. Zhu, X. Qiu, *ACS Appl. Mater. Interfaces* **2016**, *8*, 32869–32874.
[100] J. Zhai, Z. Lei, D. Rooney, H. Wang, K. Sun, *J. Power Sources* **2018**, *396*, 371–378.
[101] a) R. Kore, B. Lokhande, *J. Alloys Compd.* **2017**, *725*, 129–138; b) A. Maitra, A. K. Das, S. K. Karan, S. Paria, R. Bera, B. B. Khatua, *Ind. Eng. Chem. Res.* **2017**, *56*, 2444–2457.
[102] S. Zheng, X. Li, B. Yan, Q. Hu, Y. Xu, X. Xiao, H. Xue, H. Pang, *Adv. Energy Mater.* **2017**, *7*, 1602733.
[103] M. Zhou, F. Lu, X. Shen, W. Xia, H. He, X. Zeng, *J. Mater. Chem. A* **2015**, *3*, 21201–21210.
[104] K. Jiang, B. Sun, M. Yao, N. Wang, W. Hu, S. Komarneni, *Micropor Mesopor Mater.* **2018**, *265*, 189–194.
[105] S. Sahoo, T. T. Nguyen, J.-J. Shim, *J.Ind. Eng. Chem.* **2018**, *63*, 181–190.
[106] S. G. Mohamed, S. Y. Attia, H. H. Hassan, *Micropor Mesopor Mater.* **2017**, *251*, 26–33.
[107] Y. Tao, N. Yang, C. Liang, D. Huang, P. Wang, F. Cao, Y. Luo, H. Chen, *ChemElectroChem* **2020**.
[108] H. Li, L.-J. Wu, S.-G. Zhang, C. Yao, C.-Y. Chao, H.-W. Yue, H.-H. Fan, *J. Alloy Comp* **2020**, 155008.
[109] M. K. Aslam, S. S. A. Shah, T. Najam, S. Li, C. Chen, *J. Appl. Electrochem.* **2019**, *49*, 433–442.
[110] F. Wang, C. Wang, H. Chen, W. Zhang, R. Jiang, Z. Yan, Z. Huang, H. Zhou, Y. Kuang, *Nanotechnology* **2019**, *30*, 335701.
[111] L. Yang, Y. Wu, Y. Wu, W. Younas, J. Jia, C. Cao, *J. Energy Storage* **2019**, *23*, 363–370.
[112] Q. Yu, S. Ma, H. Zhou, J. Li, Z. Wang, Z. Tan, L. Chen, Z. Huang, C. Fu, Y. Kuang, *Int. J. Hydrog. Energy* **2019**, *44*, 1816–1826.
[113] J. Mao, D. Niu, N. Zheng, G. Jiang, W. Zhao, J. Shi, Y. Li, *ACS Sustain. Chem. Eng.* **2019**, *7*, 3424–3433.

[114] Y. Zhang, J. Ding, W. Xu, M. Wang, R. Shao, Y. Sun, B. Lin, *Chem. Eng. J.* **2020**, *386*, 124030.
[115] C. Sun, W. Pan, D. Zheng, Y. Zheng, J. Zhu, C. Liu, *ACS Omega* **2020**, *5*, 4532–4541.
[116] A. Y. Faid, H. Ismail, *Mater. Today Energy* **2019**, *13*, 285–292.
[117] S. S. Karade, S. S. Raut, H. B. Gajare, P. R. Nikam, R. Sharma, B. R. Sankapal, *J. Energy Storage* **2020**, *31*, 101622.
[118] M. S. Javed, A. J. Khan, M. Hanif, M. T. Nazir, S. Hussain, M. Saleem, R. Raza, S. Yun, Z. Liu, *Int. J. Hydrog. Energy* **2020**.
[119] M. B. Askari, P. Salarizadeh, *Int. J. Hydrog. Energy* **2020**, *45*, 27482–27491.

Manuscript received: September 29, 2020
Revised manuscript received: November 30, 2020
Accepted manuscript online: December 2, 2020
Version of record online: December 14, 2020